Methylation of Ir(III)-tetrazolato complexes: an effective route to modulate the emission outputs and to switch to antimicrobial properties.

Valentina Fiorini,[a] Ilaria Zanoni,[a,b] Stefano Zacchini,[a] Anna Luisa Costa,[b] Alejandro Hochkoeppler,[c,e] Valerio Zanotti,[a] Anna Maria Ranieri,[d] Massimiliano Massi,[d]* Alessandra Stefan[c,e]* and Stefano Stagni[a]*

a: Department of Industrial Chemistry "Toso Montanari", University of Bologna, Viale Risorgimento 4, I-40136 Bologna, Italy.

b: CNR-ISTEC- National Research Council of Italy, Institute of Science and Technology for Ceramics, Via Granarolo 64 I-48018, Faenza (RA), Italy.

c: Department of Pharmacy and Biotechnology, University of Bologna, Viale Risorgimento 4, I-40136 Bologna, Italy.

d: Nanochemistry Research Institute, Department of Chemistry, Curtin University, GPO Box U 1987, Perth, Australia 6845.

e: CSGI, University of Florence, Via della Lastruccia 3, 50019 Sesto Fiorentino (FI), Italy.

ESI – Electronic Supplementary Information

ESI-MS spettroscopy

Figure S1: ESI-MS spectrum of **[F_2IrPTZ]** (positive ions region) [M+H] = 720 m/z; $[M+Na]^+$ = 742 m/z; $[M+K]^+$ = 758 m/z, CH_3CN.

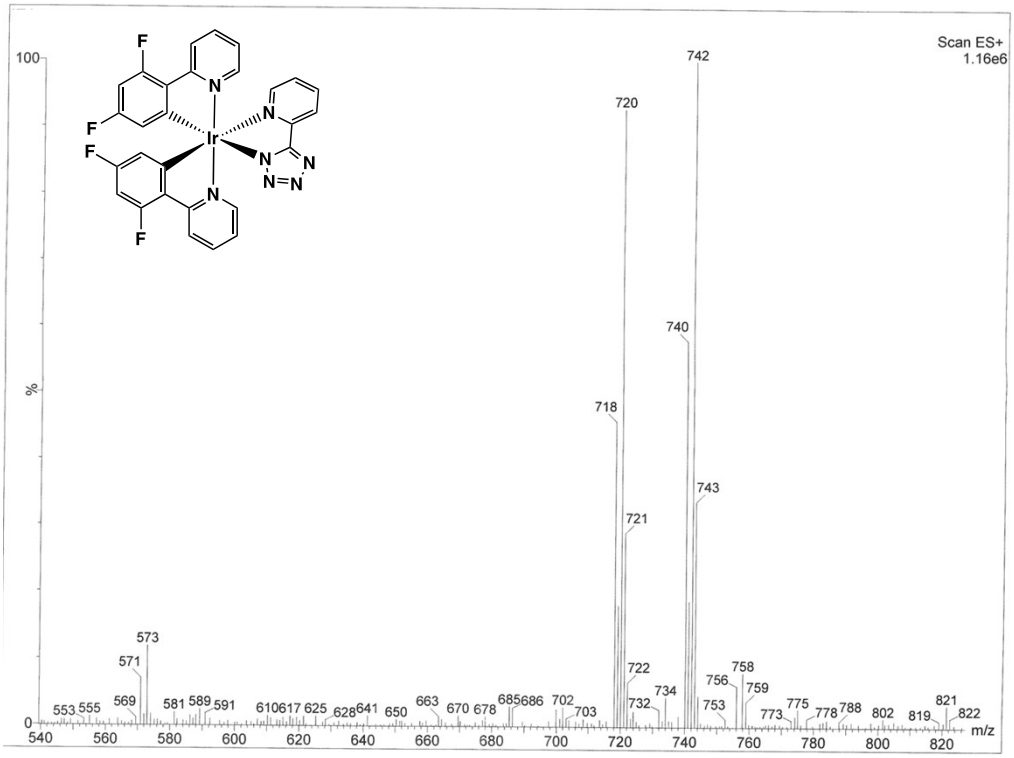

Figure S2: ESI-MS spectrum of **[F_2IrPTZ-Me]$^+$** (positive ions region) $[M]^+$ = 734 *m/z*, CH_3CN.

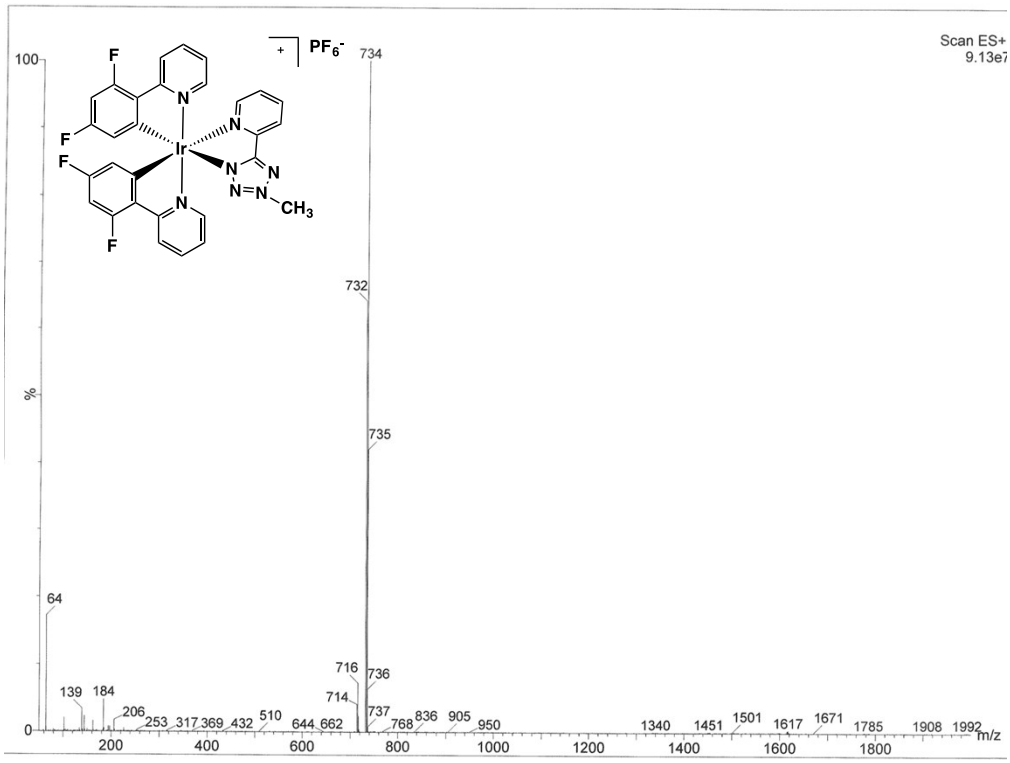

Figure S3: ESI-MS spectrum of **[IrQTZ]** positive ions region) $[M+H]^+$ = 698 *m/z*, CH_3CN.

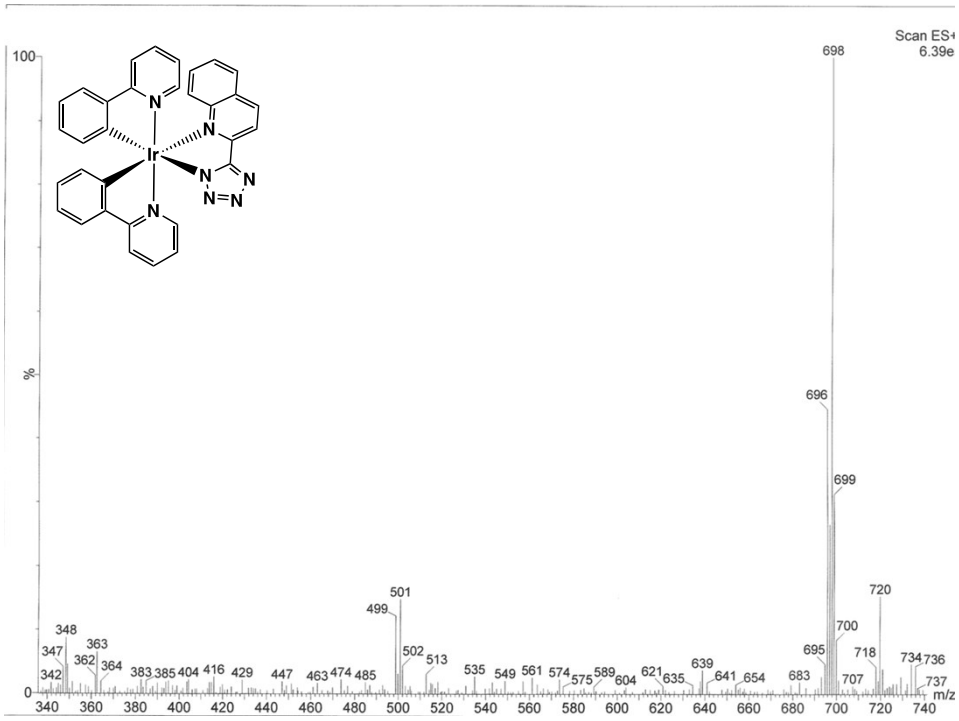

Figure S4: ESI-MS spectrum of **[IrQTZ-Me]**$^+$ positive ions region) $[M]^+$ = 712 *m/z*, CH_3CN.

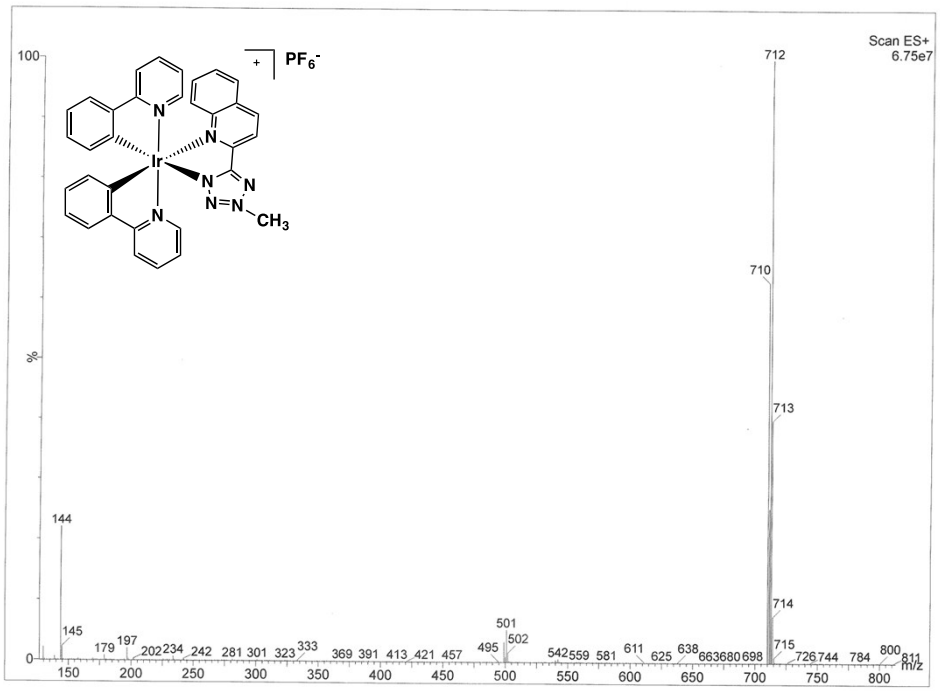

NMR spectroscopy

Figure S5: ^{1}H NMR of **[F_2IrPTZ]**, CD_3CN, 400 MHz.

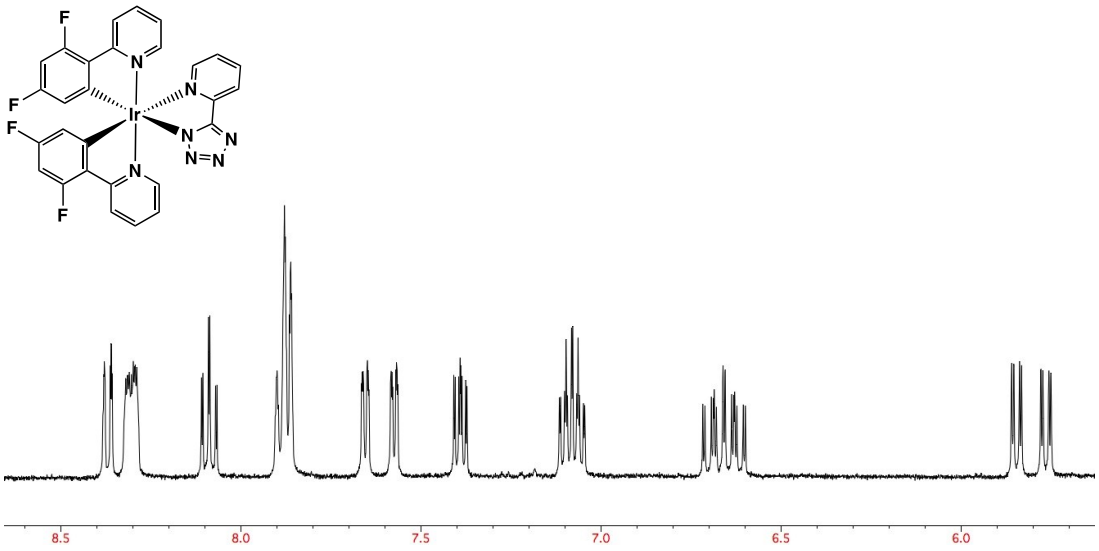

Figure S6: ^{1}H NMR of **[F_2IrPTZ-Me]$^{+}$**, CD_3CN, 400 MHz.

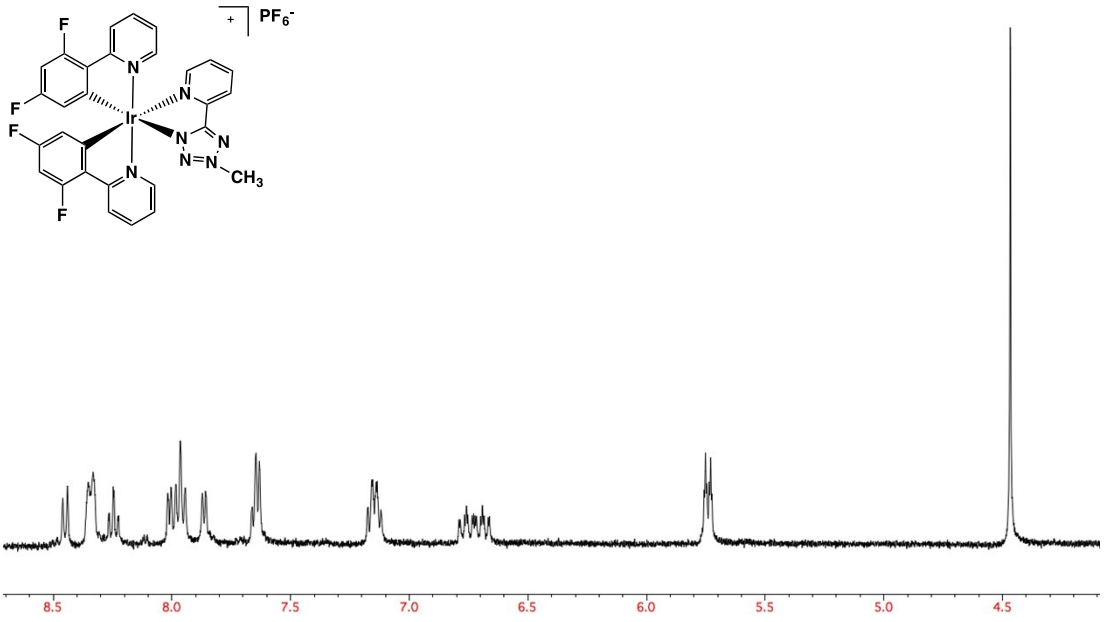

Figure S7: ^{1}H NMR of **[IrQTZ]**, CD_3CN, 400 MHz.

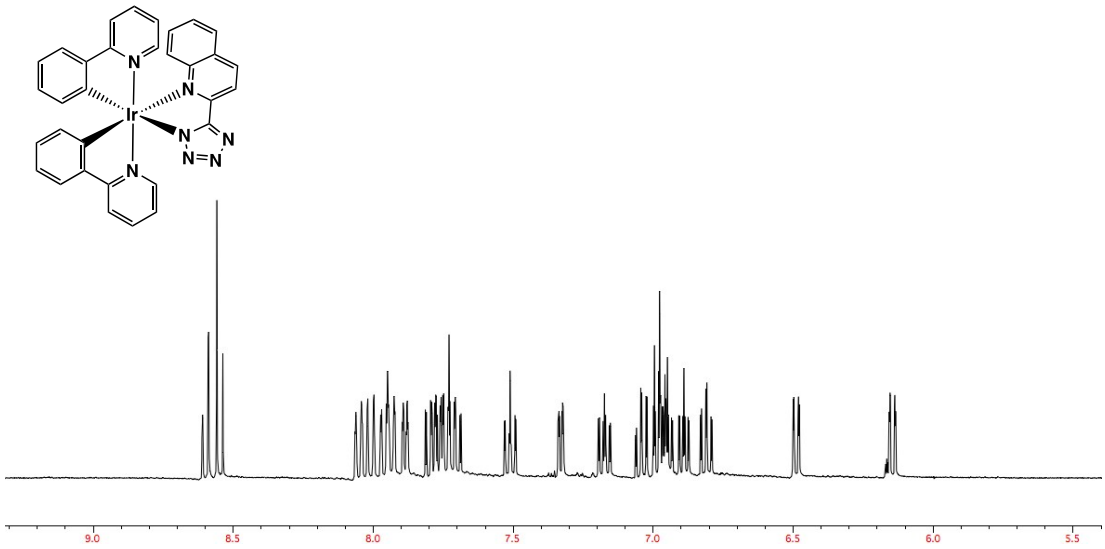

Figure S8: ^{1}H NMR of **[IrQTZ-Me]$^{+}$**, CD_3CN, 400 MHz.

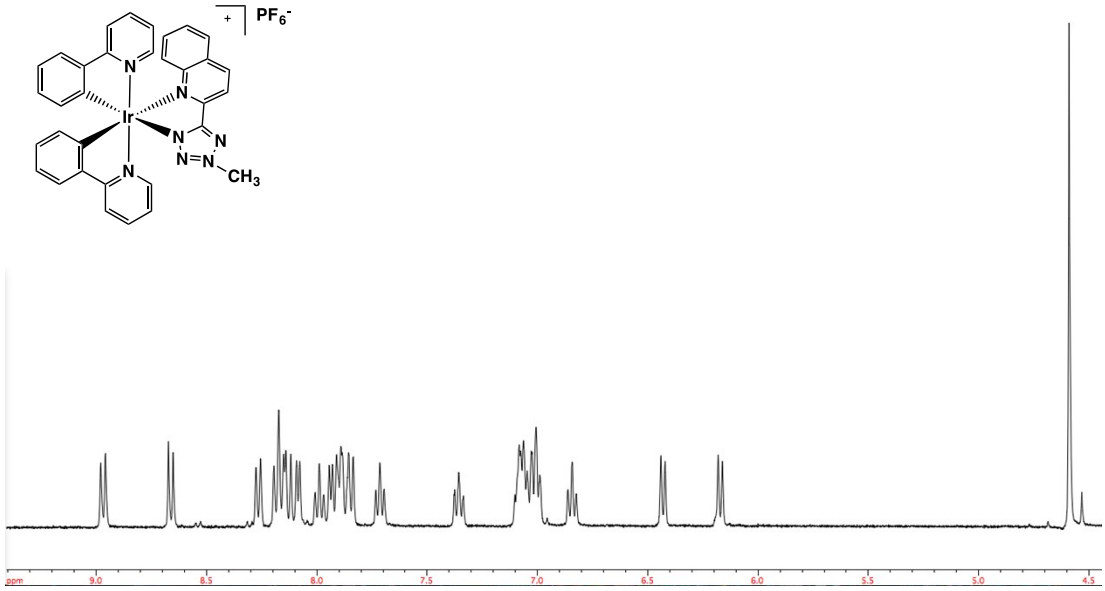

Figure S9: ^{13}C NMR of **[F_2IrPTZ]**, CD_3CN, 400 MHz.

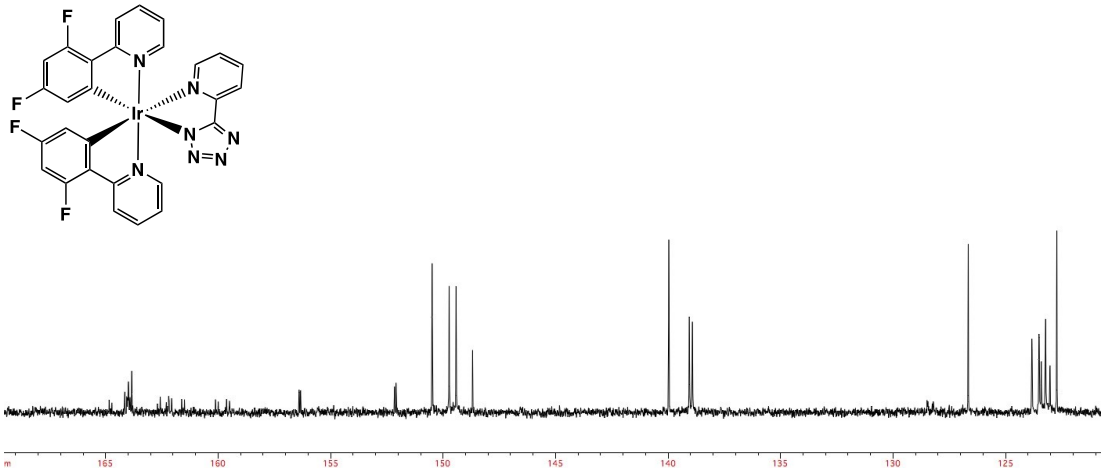

Figure S10: ^{13}C NMR of **[F_2IrPTZ-Me]$^+$**, CD_3CN, 400 MHz.

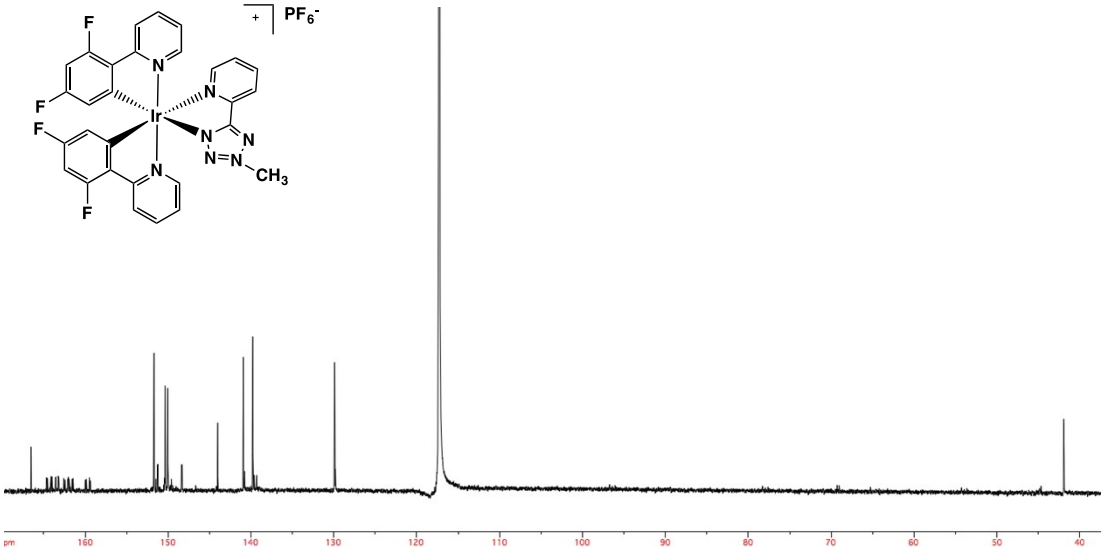

Figure S11: ^{13}C NMR of **[IrQTZ]**, CD_3CN, 400 MHz.

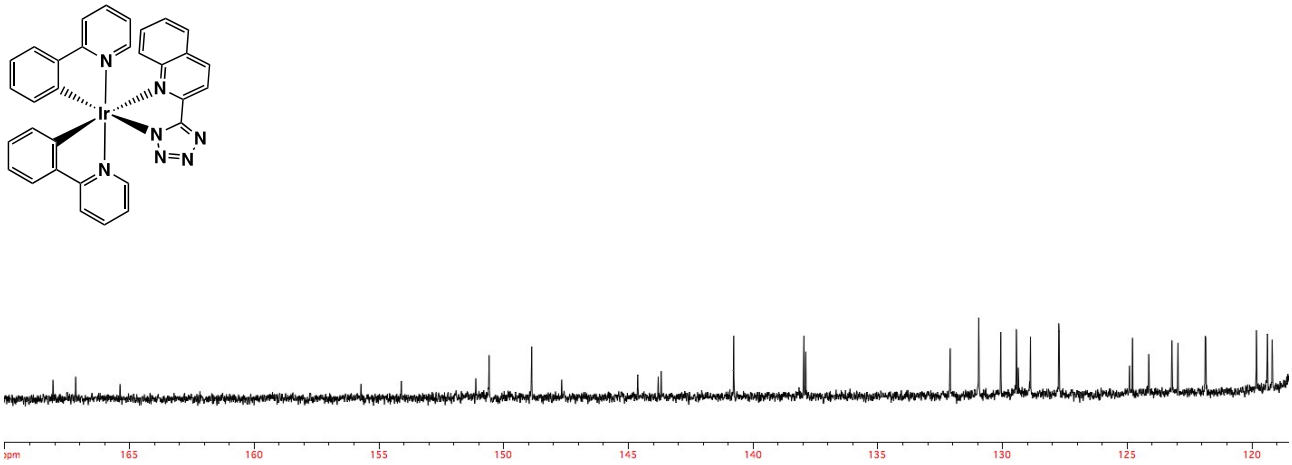

Figure S12: ^{13}C NMR of **[IrQTZ-Me]$^+$**, CD_3CN, 400 MHz.

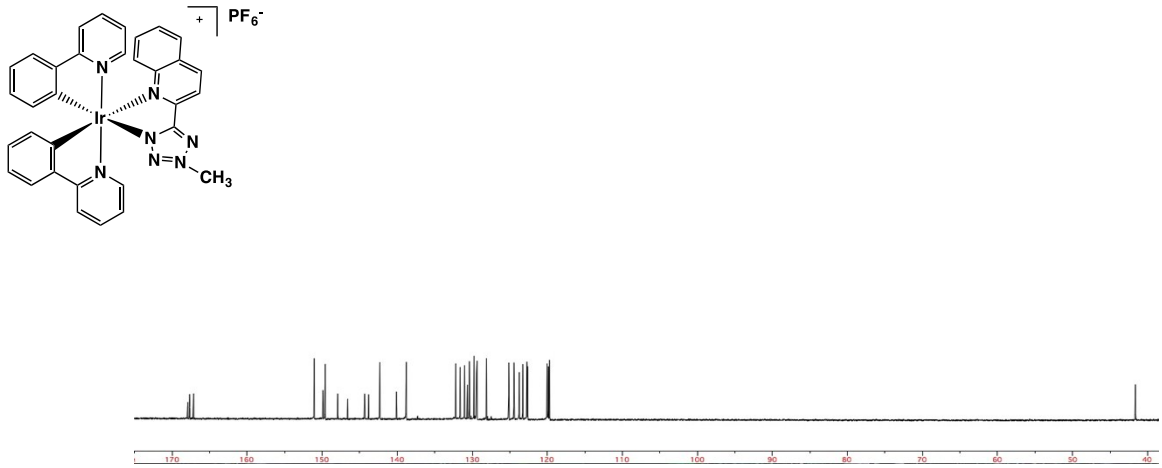

Photophysical Proprieties

Table S1: Photophysical data summary for Ir(III) complexes discussed in this work.

CH_2Cl_2 as solvent	***Absorption***	***Emission 298 K[a,b]***					***Emission 77K[c]***	
	λ_{abs}(nm);($10^{-4}\varepsilon$)($M^{-1}cm^{-1}$)	λ_{em} (nm)	τ_{air} (µs)	τ_{Ar} (µs)	φ_{air} (%)	φ_{Ar} (%)	λ_{em} (nm)	τ (µs)
[IrQTZ]	260 (6.48), 342 (1.60), 386 (0.72), 423 (0.45)	580	0.160	0.840	2.6	6.5	516, 550	4.2
[IrQTZ-Me]$^+$	253 (4.25), 310 (1.41), 374 (0.78)	638	0.220	0.550	2.8	4.5	568	1.56
[F_2IrPTZ]	252 (7.84), 304 (3.30), 369 (1.04)	456, 486	0.100	0.160	2.8	6.9	456, 486	2.69
[F_2IrPTZ-Me]$^+$	257 (6.24), 318 (2.70), 351 (1.20)	454, 486, 526	0.040	0.140	1.7	4.7	448 480	6.62

[a]: "Air" means air equilibrated solutions, "Ar" means deoxygenated solutions under argon atmosphere; [b]: $[Ru(bpy)_3]Cl_2/H_2O$ was used as reference for quantum yield determinations ($\Phi_r = 0.028$)[18]; [c]: in frozen CH_2Cl_2

Figure S13: (left) absorption profile of **[F_2IrPTZ]**, 10^{-5} M, CH_2Cl_2, r.t.; (right) excitation profile of **[F_2IrPTZ]**, 10^{-5} M, CH_2Cl_2, r.t.

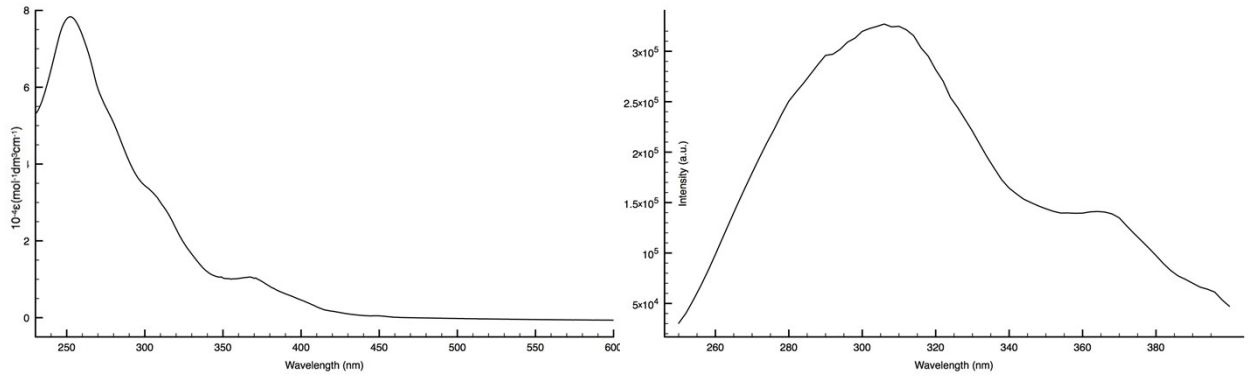

Figure S14: (left) absorption profile of **[F_2IrPTZ-Me]$^+$**, 10^{-5} M, CH_2Cl_2, r.t.; (right) excitation profile of **[F_2IrPTZ-Me]$^+$**, 10^{-5} M, CH_2Cl_2, r.t.

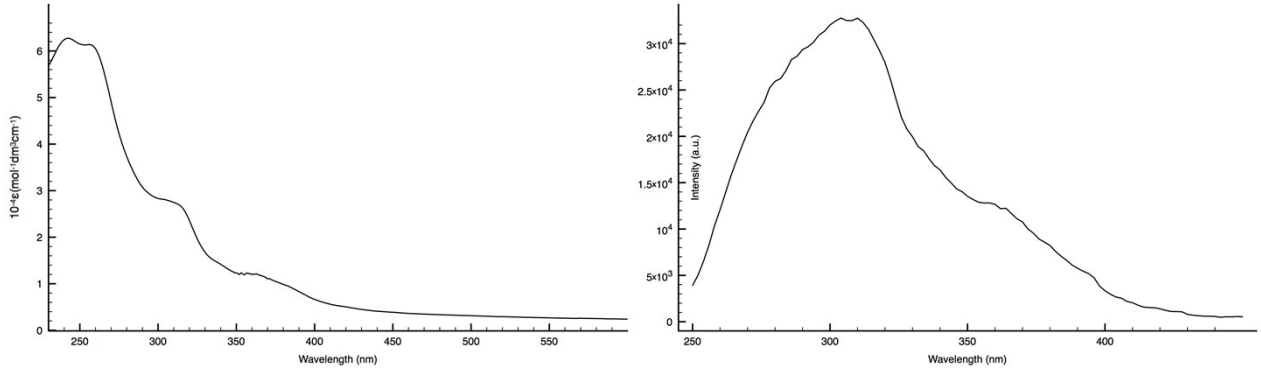

Figure S15: (left) absorption profile of **[IrQTZ]**, 10^{-5} M, CH_2Cl_2, r.t.; (right) excitation profile of **[IrQTZ]**, 10^{-5} M, CH_2Cl_2, r.t.

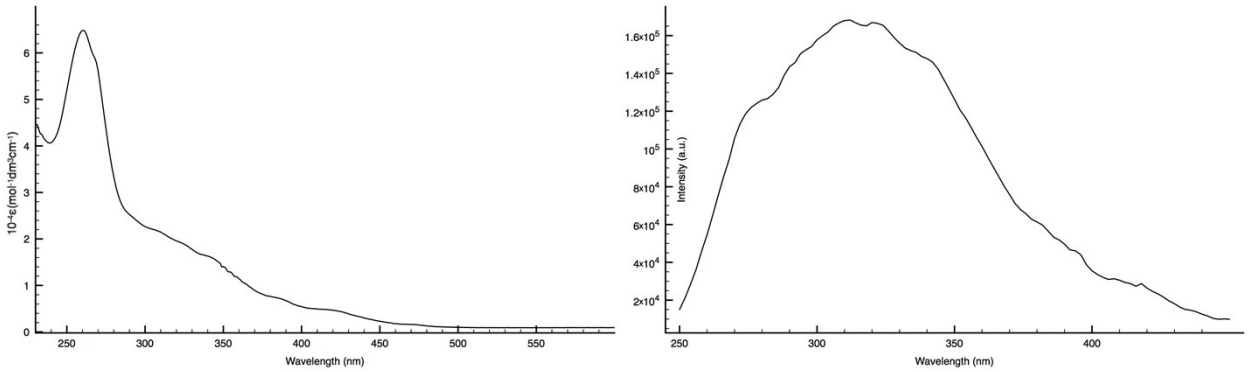

Figure S16: (left) absorption profile of **[IrQTZ-Me]**$^+$, 10^{-5} M, CH_2Cl_2, r.t.; (right) excitation profile of **[IrQTZ-Me]**$^+$, 10^{-5} M, CH_2Cl_2, r.t.

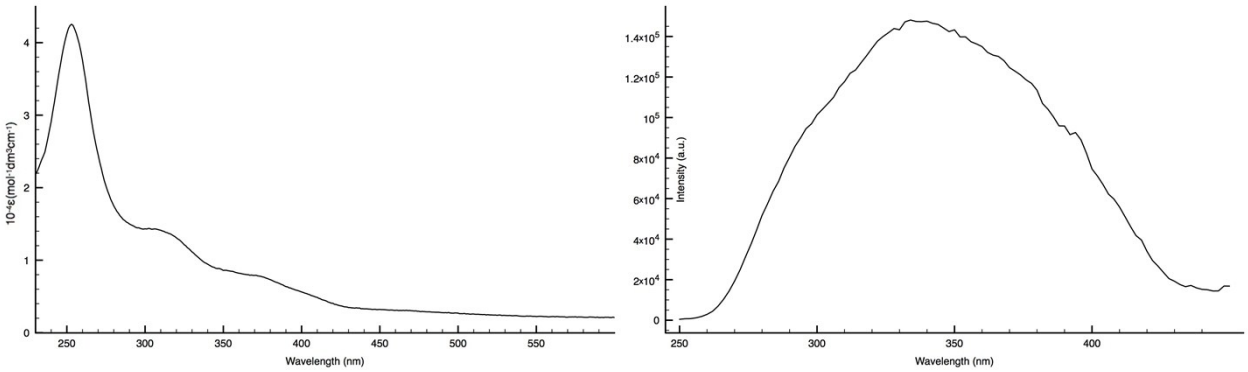

Figure S17: Emission profile of **[F_2IrPTZ]**, air equilibrated (black line) and deoxygenated solution (blue line), 10^{-5} M, CH_2Cl_2, r.t.

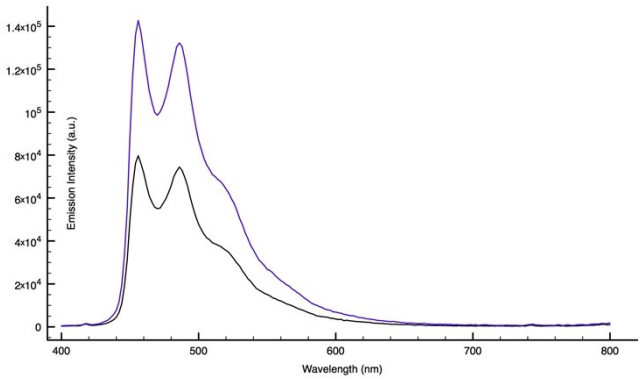

Figure S18: Emission profile of **[F_2IrPTZ]**, 298K (black line) and frozen solvent matrix, 77K (blue line), 10^{-5} M, CH_2Cl_2.

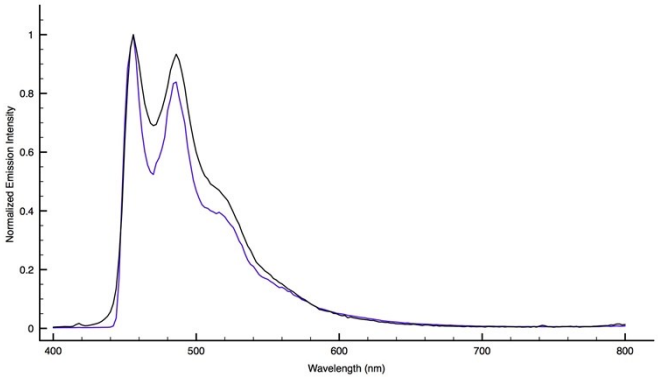

Figure S19: Emission profile of **[F_2IrPTZ-Me]$^+$**, air equilibrated (black line) and deoxygenated solution (blue line), 10^{-5} M, CH_2Cl_2, r.t.

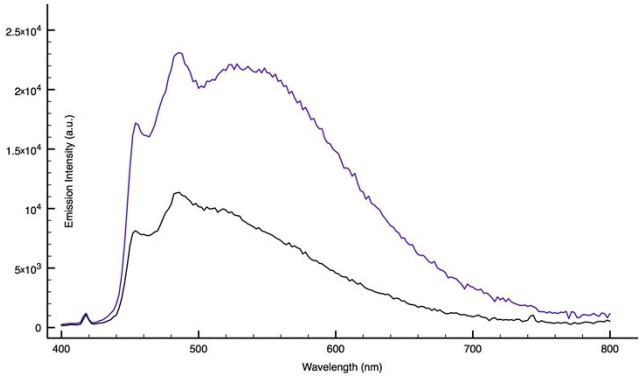

Figure S20: Emission profile of **[F_2IrPTZ-Me]$^+$**, 298K (black line) and frozen solvent matrix, 77K (blue line), 10^{-5} M, CH_2Cl_2.

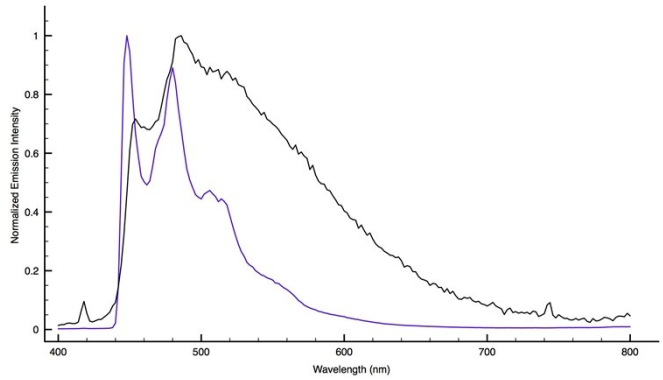

Figure S21: Normalized Emission profile of **[F_2IrPTZ]** (blue line) and **[F_2IrPTZ-Me]$^+$** (red line), 298K, 10^{-5} M, CH_2Cl_2.

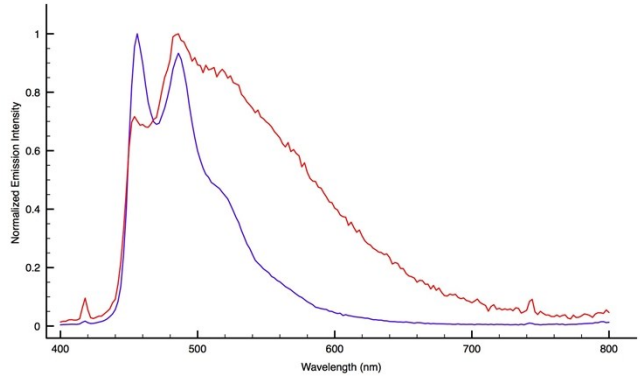

Figure S22: Emission profile of **[IrQTZ]**, air equilibrated (black line) and deoxygenated solution (blue line), 10^{-5} M, CH_2Cl_2, r.t.

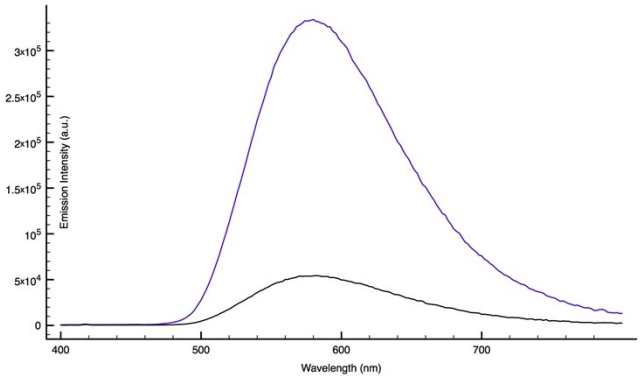

Figure S23: Emission profile of **[IrQTZ]**, 298K (black line) and frozen solvent matrix, 77K (blue line), 10^{-5} M, CH_2Cl_2.

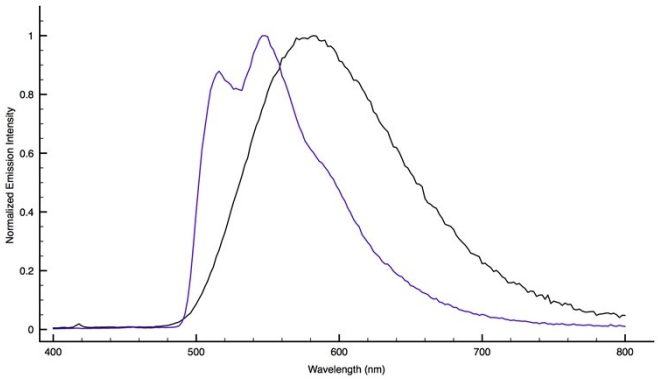

Figure S24: Emission profile of **[IrQTZ-Me]$^+$**, air equilibrated (black line) and deoxygenated solution (blue line), 10^{-5} M, CH_2Cl_2, r.t.

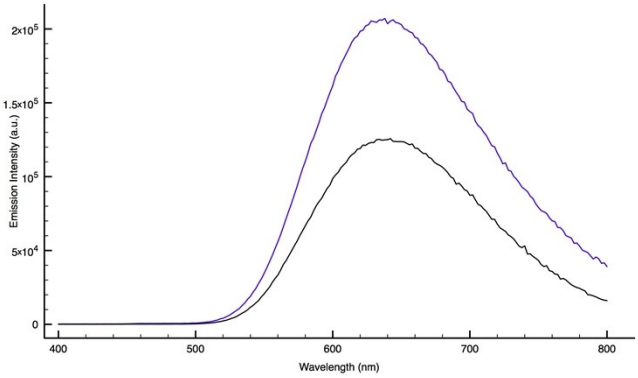

Figure S25: Emission profile of **[IrQTZ-Me]$^+$**, 298K (black line) and frozen solvent matrix, 77K (blue line), 10^{-5} M, CH_2Cl_2.

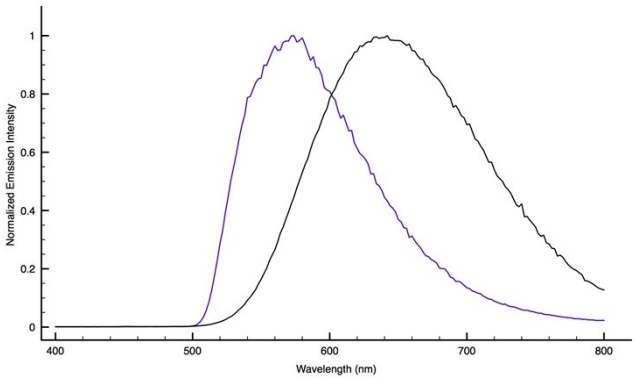

Figure S26: Normalized Emission profile of **[IrQTZ]** (blue line) and **[IrQTZ-Me]**$^{+}$ (red line), 298K, 10^{-5} M, CH_2Cl_2.

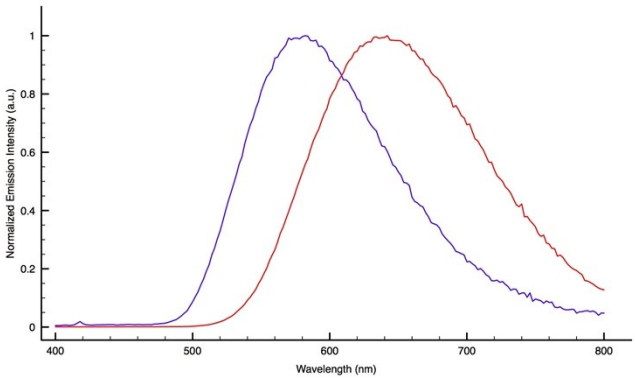

Evaluation of the antibacterial activity

Figure S27: Kinetics of growth of *Escherichia coli* at 37 °C. Cultures were incubated with 5 μM and 20 μM **[F_2IrPTZ]** and **[IrQTZ]** or with 5 μM and 20 μM **[F_2IrPTZ-Me]$^+$** and **[IrQTZ-Me]$^+$** complexes (panel a and b, respectively). A control culture (dark dots) and cultures treated with 0.4% and 1.5% DMSO are shown (green and pale green lines, respectively).

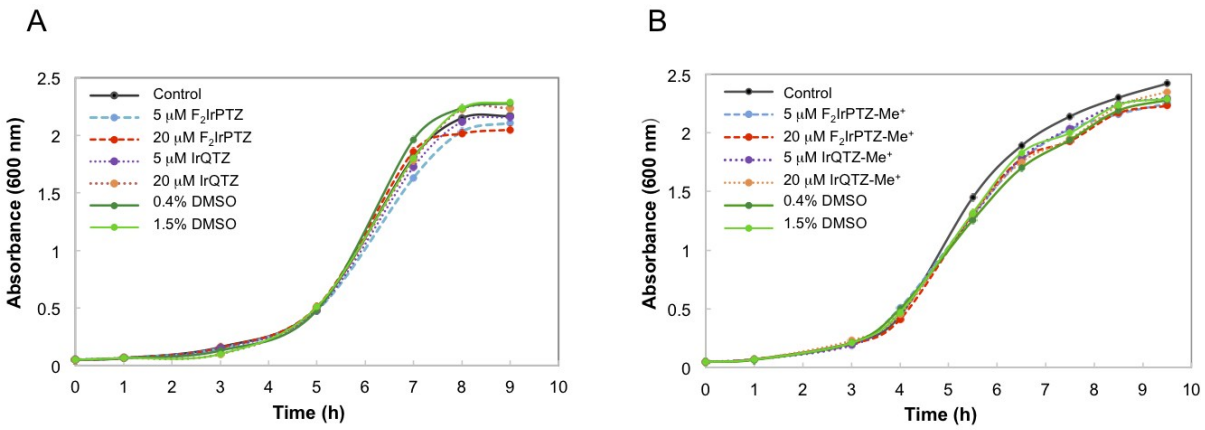

Figure S28: Kinetics of growth of *Deinococcus radiodurans* at 30 °C in the presence of neutral complexes. Cultures were treated with 5 µM and 20 µM **[F_2IrPTZ]** (a) or **[IrQTZ]** (b) (blue and red dots, respectively), 0.4% DMSO (green dots) and 1.5% DMSO (orange dots). A control culture without any complex was performed (black curve).

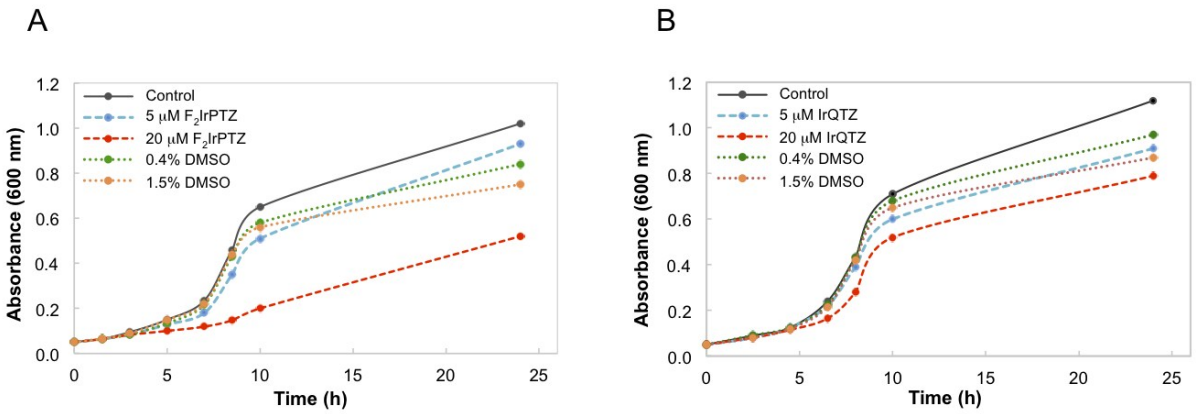

Table S2: Growth data at 30°C of of *Deinococcus radiodurans* cultures in the presence of **[F_2IrPTZ]**

Time	Absorbance at 600 nm				
	Control	**5µM [F_2IrPTZ]**	**20 µM [F_2IrPTZ]**	**0.4% DMSO**	**1.5% DMSO**
0	0.05	0.05	0.05	0.05	0.05
1.5	0.065	0.064	0.064	0.065	0.065
3	0.095	0.0855	0.083	0.085	0.089
5	0.15	0.128	0.1	0.134	0.149
7	0.235	0.18	0.119	0.216	0.22
8.5	0.46	0.35	0.147	0.43	0.44
10	0.65	0.51	0.2	0.58	0.56
24	1.02	0.93	0.52	0.84	0.75

Table S3: Growth data at 30°C of of *Deinococcus radiodurans* cultures in the presence of **[IrQTZ]**

Time	Absorbance at 600 nm				
	Control	**5µM [IrQTZ]**	**20 µM [IrQTZ]**	**0.4% DMSO**	**1.5% DMSO**
0	0.05	0.05	0.05	0.05	0.05
2.5	0.09	0.08	0.081	0.091	0.08
4.5	0.125	0.125	0.115	0.125	0.12
6.5	0.24	0.22	0.165	0.225	0.215
8	0.435	0.39	0.28	0.43	0.42
10	0.71	0.6	0.52	0.68	0.65
24	1.12	0.91	0.79	0.97	0.87

Figure S29: Kinetics of growth of *Deinococcus radiodurans* at 30 °C in the presence of cationic complexes. Cultures were treated with 5 µM and 20 µM **[F_2IrPTZ-Me]$^+$**(a) or **[IrQTZ-Me]$^+$**(b) (blue and red dots, respectively), 0.4% DMSO (green dots) and 1.5% DMSO (orange dots). A control culture without any complex was performed (black curve).

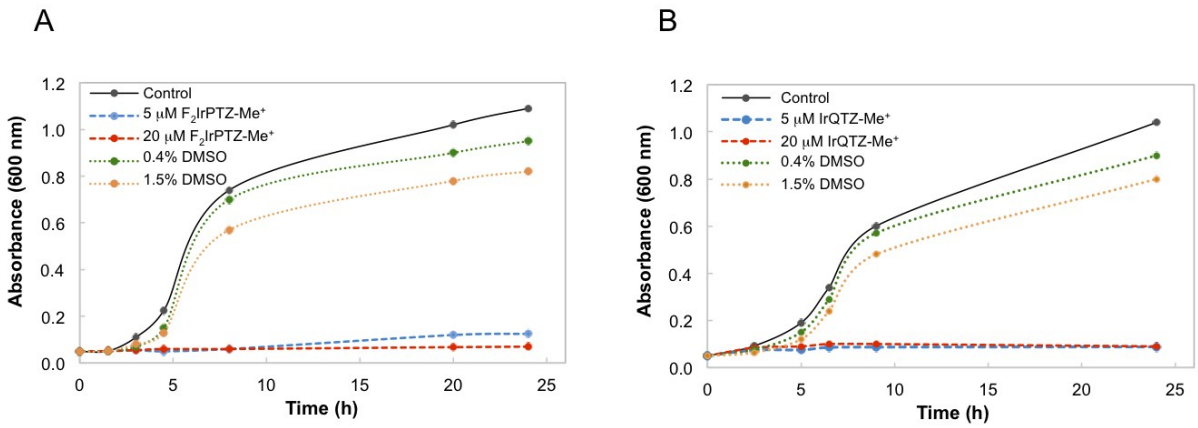

Table S4: Growth data at 30°C of of *Deinococcus radiodurans* cultures in the presence of **[F_2IrPTZ-Me]$^+$**

Time	Absorbance at 600 nm				
	Control	5µM [F_2IrPTZ-Me]$^+$	20 µM [F_2IrPTZ-Me]$^+$	0.4% DMSO	1.5% DMSO
0	0.05	0.05	0.05	0.05	0.05
1.5	0.051	0.051	0.051	0.051	0.051
3	0.11	0.055	0.055	0.07	0.08
4.5	0.225	0.05	0.06	0.15	0.13
8	0.74	0.06	0.06	0.7	0.57
20	1.02	0.12	0.068	0.9	0.78
24	1.09	0.125	0.07	0.95	0.82

Table S5: Growth data at 30°C of of *Deinococcus radiodurans* cultures in the presence of **[IrQTZ-Me]$^+$**

Time	Absorbance at 600 nm				
	Control	5µM [IrQTZ-Me]$^+$	20 µM [IrQTZ-Me]$^+$	0.4% DMSO	1.5% DMSO
0	0.05	0.05	0.05	0.05	0.05
2.5	0.092	0.074	0.084	0.076	0.064
5	0.19	0.075	0.09	0.15	0.12
7	0.33	0.086	0.1	0.29	0.24
9	0.60	0.087	0.1	0.57	0.48
24	1.04	0.088	0.09	0.9	0.8

Figure S30: Kinetics of growth of *Deinococcus radiodurans* at 30 °C in the presence of different concentration of cationic complexes. Cultures were treated with 0.5, 1, 2.5 and 5 µM **[F_2IrPTZ-Me]$^+$** or **[IrQTZ-Me]$^+$** (a and b, respectively). A control culture without any complex was performed (black curve).

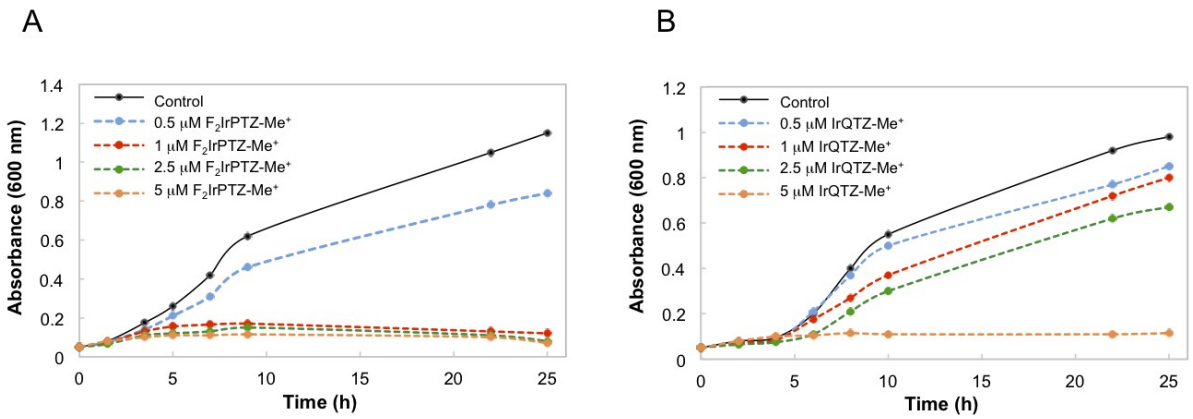

Figure S31: Kinetics of growth of *Deinococcus radiodurans* at 30 °C in the presence of different concentration of neutral **[IrPTZ]** complex. Cultures were treated with 5 µM and 20 µM (blue dots and red dots, respectively) 0.4% DMSO (green dots) and 1.5% DMSO (orange dots). A control culture without any complex was performed (black curve).

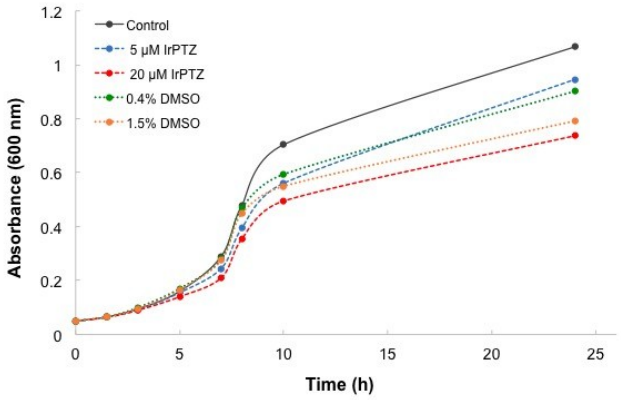

Table S6: Growth data at 30°C of of *Deinococcus radiodurans* cultures in the presence of **[IrPTZ]**.

Time	Absorbance at 600 nm				
	Control	**5µM [IrPTZ]**	**20 µM [IrPTZ]**	**0.4% DMSO**	**1.5% DMSO**
0	0.05	0.05	0.05	0.05	0.05
1.5	0.065	0.064	0.064	0.065	0.065
3	0.095	0.092	0.09	0.1	0.095
5	0.16	0.155	0.14	0.17	0.165
7	0.29	0.245	0.21	0.28	0.275
8	0.48	0.395	0.355	0.47	0.45
10	0.704	0.561	0.495	0.594	0.55
24	1.067	0.946	0.737	0.902	0.792

Figure S32: kinetics of dark-growth of *Deinococcus radiodurans* at 30 °C, in the presence of different concentration of cationic complexes. Cultures were treated with 5 and 20 µM **[F_2IrPTZ-Me]$^+$** or **[IrQTZ-Me]$^+$** (blue dots/red dots, green dots/orange dots, respectively). A control culture without any complex was performed (black curve).

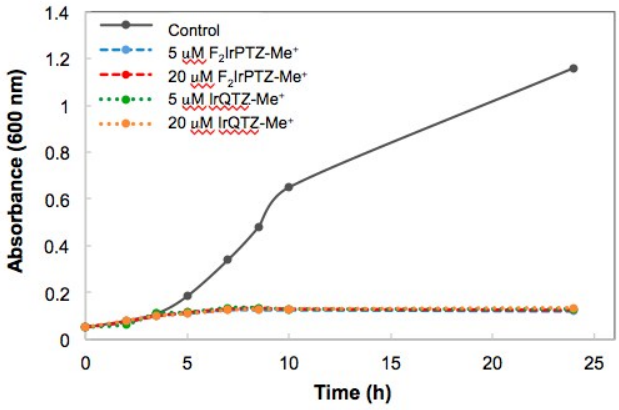

Table S7: dark-growth data at 30°C of *Deinococcus radiodurans* cultures in the presence of **[F_2IrPTZ-Me]$^+$** and **[IrQTZ-Me]$^+$**.

Time	Absorbance at 600 nm				
	Control	**5µM [F_2IrPTZ-Me]$^+$**	**20 µM [F_2IrPTZ-Me]$^+$**	**5µM [IrQTZ-Me]$^+$**	**20µM [IrQTZ-Me]$^+$**
0	0.05	0.05	0.05	0.05	0.05
2	0.08	0.075	0.075	0.065	0.08
3.5	0.11	0.1	0.1	0.1	0.1
5	0.185	0.11	0.115	0.17	0.11
7	0.34	0.125	0.13	0.28	0.125
8.5	0.48	0.125	0.135	0.47	0.13
10	0.65	0.125	0.13	0.594	0.13
24	1.16	0.12	0.125	0.902	0.135

Table S8: Crystal data and collection details for **[IrQTZ]·3CH$_3$CN**, **[IrQTZ-Me]$^+$[PF$_6$]$^-$·solv** and **[F$_2$IrPTZ-Me]$^+$[PF$_6$]$^-$·2CH$_2$Cl$_2$**.

	[IrQTZ]·3 CH$_3$CN	**[IrQTZ-Me]$^+$[PF$_6$]$^-$·solv**	**[F$_2$IrPTZ-Me]$^+$[PF$_6$]$^-$ ·2CH$_2$Cl$_2$**
Formula	$C_{38}H_{31}IrN_{10}$	$C_{33}H_{25}F_6IrN_7P$	$C_{31}H_{23}Cl_4F_{10}IrN_7P$
Fw	819.93	856.77	1048.53
T, K	100(2)	100(2)	100(2)
λ, Å	0.71073	0.71073	0.71073
Crystal system	Monoclinic	Monoclinic	Monoclinic
Space Group	$P2_1/n$	$P2_1/c$	$P2_1/c$
a, Å	10.1798(7)	8.4719(5)	16.992(3)
b, Å	21.5492(15)	18.6483(10)	11.9864(19)
c, Å	15.7661(11)	41.050(2)	17.811(3)
β, °	98.325(2)	93.604(4)	96.203(3)
Cell Volume, Å^3	33422.1(4)	6472.5(6)	3606.3(10)
Z	4	8	4
D_c, g cm^{-3}	1.591	1.758	1.931
μ, mm^{-1}	3.945	4.246	4.131
F(000)	1624	3344	2032
Crystal size, mm	0.22×0.18×0.14	0.14×0.11×0.07	0.14×0.12×0.10
θ limits, °	1.612–28.000	1.477–23.531	2.052–25.100
Index ranges	-13 ≤ h ≤ 13 -28 ≤ k ≤ 28 -20 ≤ l ≤ 20	-9 ≤ h ≤9 -20 ≤ k ≤ 20 -46 ≤ l ≤46	-20 ≤ h ≤20 -14 ≤ k ≤ 14 -421 ≤ l ≤ 21
Reflections collected	50767	61336	39761
Independent reflections	8272 [R_{int} = 0.0383]	9620 [R_{int} = 0.3090]	6406 [R_{int} = 0.0730]
Completeness to θ max	100.0%	100.0%	99.08%
Data / restraints / parameters	8272 / 105 / 456	9620 / 1008 / 866	6406 / 494 / 439
Goodness on fit on F^2	1.073	1.026	1.078
R_1 (I> 2σ(I))	0.0219	0.0817	0.0857
wR_2 (all data)	0.0530	0.1826	0.2325
Largest diff. peak and hole, e Å^{-3}	0.908 / –1.388	1.291 / –2.043	3.815 / –2.533